



The Stonehenge Altar Stone was probably not sourced from the Old Red Sandstone of the Anglo-Welsh Basin: Time to broaden our geographic and stratigraphic horizons?

Richard E. Bevins^{a,*}, Nick J.G. Pearce^a, Rob A. Ixer^b, Duncan Pirrie^c, Sergio Andò^d, Stephen Hillier^{e,f}, Peter Turner^g, Matthew Power^h

^a Department of Geography and Earth Sciences, Aberystwyth University, Aberystwyth SY23 3DB, UK

^b Institute of Archaeology, University College London, London WC1H 0PY, UK

^c Faculty of Computing, Engineering and Science, University of South Wales, Pontypridd CF37 4BD, UK

^d Department of Earth and Environmental Sciences, Università degli Studi di Milano-Bicocca, 20126 Milano, Italy

^e The James Hutton Institute, Craigiebuckler, Aberdeen AB15 8QH, UK

^f Department of Soil and Environment, Swedish University of Agricultural Sciences (SLU), SE-75007 Uppsala, Sweden

^g 7 Carlton Croft, Streeley, West Midlands B74 3JT, UK

^h Vidence Inc., 4288 Lozells Avenue, Suite 213 – L, Burnaby, British Columbia, V5A 0C7, Canada

ARTICLE INFO

Keywords:

Neolithic
Stonehenge
Altar Stone
Sandstone analysis
Provenancing

ABSTRACT

Stone 80, the recumbent Altar Stone, is the largest of the Stonehenge foreign “bluestones”, mainly igneous rocks forming the inner Stonehenge circle. The Altar Stone’s anomalous lithology, a sandstone of continental origin, led to the previous suggestion of a provenance from the Old Red Sandstone (ORS) of west Wales, close to where the majority of the bluestones have been sourced (viz. the Mynydd Preseli area in west Wales) some 225 km west of Stonehenge. Building upon earlier investigations we have examined new samples from the Old Red Sandstone (ORS) within the Anglo-Welsh Basin (covering south Wales, the Welsh Borderland, the West Midlands and Somerset) using traditional optical petrography but additionally portable XRF, automated SEM-EDS and Raman Spectroscopic techniques. One of the key characteristics of the Altar Stone is its unusually high Ba content (all except one of 106 analyses have Ba > 1025 ppm), reflecting high modal baryte. Of the 58 ORS samples analysed to date from the Anglo-Welsh Basin, only four show analyses where Ba exceeds 1000 ppm, similar to the lower range of the Altar Stone composition. However, because of their contrasting mineralogies, combined with data collected from new automated SEM-EDS and Raman Spectroscopic analyses these four samples must be discounted as being from the source of the Altar Stone. It now seems ever more likely that the Altar Stone was not derived from the ORS of the Anglo-Welsh Basin, and therefore it is time to broaden our horizons, both geographically and stratigraphically into northern Britain and also to consider continental sandstones of a younger age. There is no doubt that considering the Altar Stone as a ‘bluestone’ has influenced thinking regarding the long-held view to a source in Wales. We therefore propose that the Altar Stone should be ‘de-classified’ as a bluestone, breaking a link to the essentially Mynydd Preseli-derived bluestones.

1. Introduction

Stonehenge is arguably the most iconic of Neolithic monuments in the World. It stands on Salisbury Plain in Wiltshire and [Parker Pearson \(2023, 161\)](#) considers that it was first erected in the Late Neolithic around 3000 BCE. The initial phase of construction was followed by four further re-modelling phases, the last being in the Middle Bronze Age, ca.

1600 BCE. It was during the first phase that according to Parker Pearson (op. cit.) the bluestones were erected as a single ring of stones set in a series of 56 pits known as the Aubrey Holes. [Pitts \(2022\)](#) called this ring of stones ‘bluehenge’. The larger sarsen stones are thought to have been brought to Stonehenge during construction Phase 2, at the end of the Late Neolithic (ca. 2500 BCE). However, other authors have alternative chronologies for Stonehenge; see for example [Darvill \(2022\)](#), who also

* Corresponding author.

E-mail address: rib24@aber.ac.uk (R.E. Bevins).

<https://doi.org/10.1016/j.jasrep.2023.104215>

Received 27 June 2023; Received in revised form 30 August 2023; Accepted 14 September 2023

Available online 22 September 2023

2352-409X/Crown Copyright © 2023 Published by Elsevier Ltd.

This is an open access article under the CC BY-NC-ND license

(<http://creativecommons.org/licenses/by-nc-nd/4.0/>).

questions whether the Aubrey Holes ever held bluestone monoliths.

The bluestones, predominantly of igneous origin, were termed the ‘Foreign Stones’ by early excavators at Stonehenge (for example [Cunnington, 1884](#)), being exotic to the Wiltshire landscape, in contrast to the sarsen stones, which are identified as being of relatively local derivation, [Nash et al. \(2020\)](#) recently stating that the principal source of the Stonehenge sarsens was most likely West Woods, ca. 25 km north of Stonehenge. The majority of the bluestones have been sourced to the Mynydd Preseli area in west Wales (see [Figure 1](#)), ca. 225 km west of Stonehenge, originally by [Thomas \(1923\)](#) and with more recent investigations by [Thorpe et al., \(1991\)](#), ([Ixer and Bevins 2010](#); [Ixer and Bevins 2011](#)), ([Bevins et al. 2012](#); [Bevins et al. 2014](#); [Bevins et al. 2021](#)) and [Pearce et al. \(2022\)](#).

Monoliths used in the construction of stone circles are usually locally derived. [Linares-Catela et al. \(2023\)](#) recently reported that stones used in the El Pozuelo megalithic complex in Huelva, Spain were moved from distances in the range of 50–350 m. One of the best documented examples from the Neolithic of Britain is the sourcing of stones used in the Ring of Brodgar and the Stones of Stenness monuments on Orkney in north Scotland which were quarried from sources around Staneyhill and Vestra Fiold, no more than 5–10 km away ([Downes et al., 2013](#); [Richards et al., 2013](#)). It is the long-distance transport of the bluestones that makes Stonehenge of particular interest; the bluestones in fact represent one of the longest transport distances known from source to monument construction site anywhere in the world ([Parker Pearson et al., 2020](#)).

Through the recent studies mentioned above there has been a continued refinement of the Preseli sources of some of the bluestone lithologies, including Craig Rhos-y-Felin (the source of the main rhyolitic debitage at Stonehenge and possibly the buried stump of Stone 32d), Carn Goedog (the main source of the spotted dolerites) and Garn

Ddu Fach (the source of the non-spotted dolerite Stone 62). One bluestone, Stone 80, known as the Altar Stone, a grey-green (on fresh surfaces), micaceous sandstone, however, is anomalous in that it is not derived from the Mynydd Preseli and surrounding area, and it is this stone that is the subject of this paper.

2. Previous work and scope of this paper

As noted by [Bevins et al. \(2022a\)](#), one of the earliest references to the Altar Stone was in a letter from Professor John Phillips of Oxford University to archaeologist Dr John Thurnam in 1858, suggesting that it might have been sourced in the ‘...Devonian or gray Cambrian rocks.’, possibly referring to the marine Devonian sequences in southwest England. [Maskelyne \(1878\)](#) mentioned this attribution but noted that his assistant, Mr Thomas Davies, had informed him that such rocks could be found in the Frome area, in the Mendips of Somerset. [Thomas \(1923\)](#) considered that the Altar Stone is of Old Red Sandstone (ORS) age and might have been derived from outcrops in west or south Wales lying to the south or east of the Mynydd Preseli, either from beds of the Coshston Group (now called the Cosheston Subgroup) or the Senni Beds (now called the Senni Formation).

The Altar Stone is the largest of all the bluestones, measuring 4.9 m long by 1 m wide by 0.5 m thick with a slab-like form. Recent investigations by [Ixer et al. \(2019\)](#) and ([Bevins et al. 2020](#); [Bevins et al. 2022a](#); [Bevins et al. 2023](#)) have attempted to provenance the Altar Stone by characterizing its chemistry and mineralogy using a range of analytical techniques, in particular automated scanning electron microscopy (SEM-EDS), U-Pb zircon age determination and preliminary portable X-ray fluorescence (pXRF) analysis. Key characteristics include abundant mica, heavy mineral laminae defining ripple bedforms, the

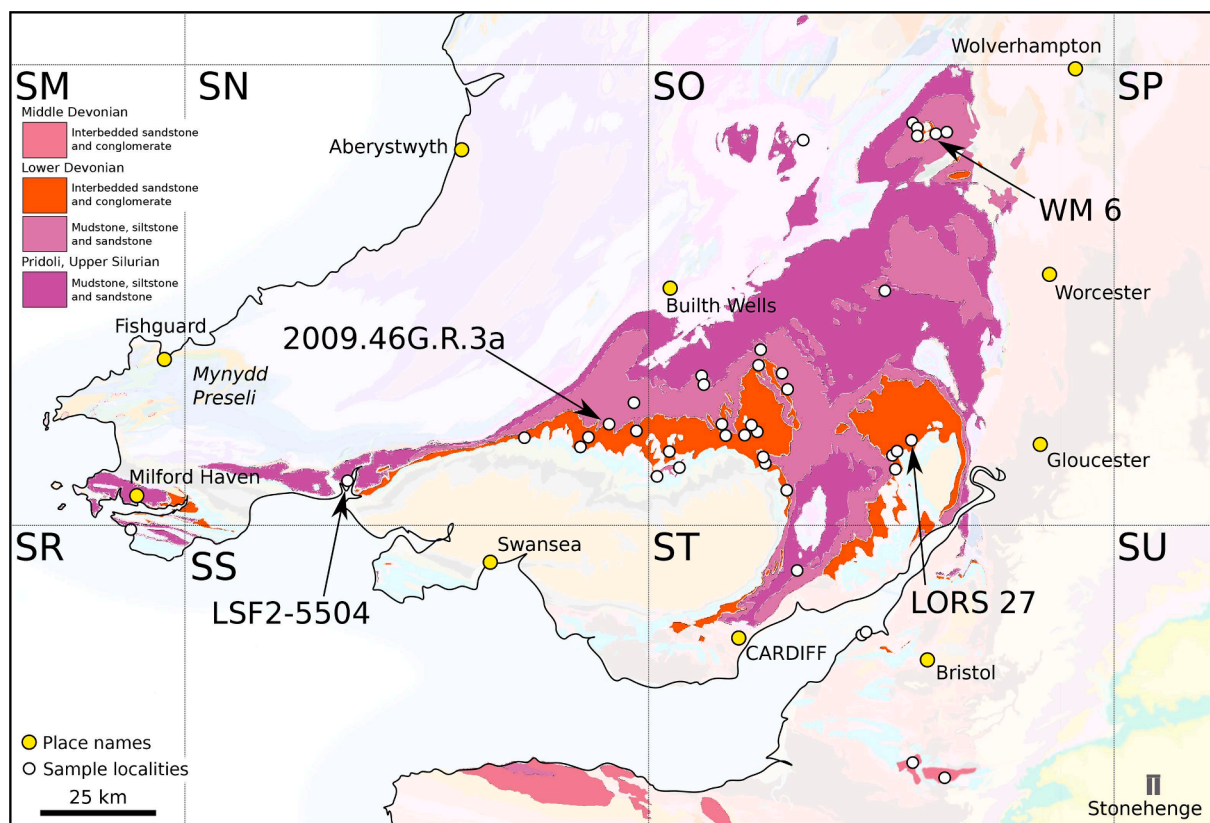


Fig. 1. Location map for samples analysed in this study, including the outcrop map of Old Red Sandstone sedimentary strata in the Anglo-Welsh Basin (bolder colours) overlain on the background geological map of the area (faded colours). Contains British Geological Survey materials © UKRI [2023] from BGS GeIndex (onshore). Grid lines mark the British National Grid 100 km squares, designated by their 2-letter code (e.g. SN, see [Supplementary Table 1](#)). The location of Stonehenge is shown at the bottom right of the map. The locations of the four high Ba ORS samples are indicated by their sample numbers.

presence of early formed pore-filling baryte and kaolinite cement, thought to be linked to burial diagenesis, a later calcite cement which post-dates quartz overgrowths which occludes much of the available porosity and a near absence of K feldspar. The presence of baryte is reflected in the high Ba contents as determined through the pXRF investigations presented in Bevins et al. (2022a, 2023), with the average composition from all *in situ* analyses of the Altar Stone exceeding 2750 ppm.

Bevins et al. (2022a), on the basis of their preliminary pXRF analyses and limited automated mineralogy data, were unable to offer any potential source for the Altar Stone and remarked that they needed to ‘keep an open mind over the potential source of the Altar Stone, especially as we are not aware of any reports of baryte-bearing sandstones in the Old Red Sandstone sequences of Wales and the Welsh Borderland’. This paper reports on the findings of further, continuing investigations of the Old Red Sandstone (ORS) in Wales, the Welsh Borderland and the West Midlands and Somerset in England (in the Anglo-Welsh Basin of Barclay et al., 2015) based on an enlarged pXRF database, further automated SEM-EDS analyses and initial findings of Raman Spectroscopy analyses of an Altar Stone fragment and an ORS sample from the West Midlands which bears certain geochemical and mineralogical similarities to the Altar Stone. The perspective we are forming is that it is perhaps time to broaden our horizons, both geographically and stratigraphically, by looking elsewhere other than the ORS Anglo-Welsh Basin (see Barclay et al., 2005; Kendall, 2017 for the distribution of ORS strata in Britain) and perhaps also to consider potential sources in younger sequences of Permo-Triassic age.

3. Portable XRF analyses

In previous studies we have reported on portable XRF (pXRF) analyses of the Altar Stone (*in situ* analyses performed on two separate visits), analyses of six small pieces of debitage (which were confirmed to be fragments of the Altar Stone; Bevins et al., 2022a), and of sample 2010 K 240 from the collections of Salisbury Museum (sometimes referred to as Wilts 277), which we confirmed as a piece collected from the underside of the Altar Stone in 1844 (Bevins et al., 2023). During our studies, and subsequently, we have analysed a total of 58 geographically widespread samples of Old Red Sandstone from the Anglo-Welsh Basin in an attempt to find samples with a mineralogy and chemistry comparable with the Altar Stone (see Figure 1). The samples were drawn largely from the set used by Hillier et al. (2006) in their X-ray diffraction study of the ORS of the UK, supplemented by samples drawn from the collections of the National Museum of Wales and a small number of field-collected samples. Sample site details are presented in Supplementary Table 1.

3.1. Analytical methods

All analyses were performed using a Thermo Fisher Scientific™ Niton™ XL3t Gold+ handheld XRF analyser. The Niton pXRF uses a 2 W Ag anode X-ray tube, which can operate at between 6 and 50 kV and 0–200 μ A, with operating conditions being varied during the “Test-AllGeo” analysis method. The instrument can determine a range of elements in geological materials from Mg to U by use of different filters which operate in sequence together to optimise sensitivity, although light element analyses are less accurate without a He flush of the instrument and are sensitive to the presence of moisture in the sample. The total analysis time was 100 s, divided between four operating modes (Main range 30 s, Low range 30 s, High range 20 s, Light range 20 s) using an 8 mm diameter analysis spot to give an analysed area of ~ 50 mm², with the spectra collected on a silicon drift detector, processed and calibrated by the instrument’s manufacturer-installed calibration. Here, across several separate periods of analyses, we performed five analyses of the weathered surfaces of each ORS sample and monitored instrument calibration using a piece of the Big Obsidian Flow from

the Newbery Volcano in Oregon. All analyses are presented in the Supplementary Table 2. Elsewhere we have discussed at length analytical methods and instrument accuracy, and these aspects of the method are not revisited here (see Bevins et al., 2022a; Bevins et al., 2022b; Pearce et al., 2022; Bevins et al., 2023).

3.2. Portable XRF comparisons

Fig. 2 shows a series of bivariate plots for the data for the ORS samples from the Anglo-Welsh Basin compared with the analyses of the Altar Stone (*sensu lato*, i.e., including the debitage fragments and 2010 K 240 shown to be derived from the Altar Stone). Here we concentrate on those elements which are reported in most analyses, and which are generally determined with good accuracy by pXRF (Bevins et al., 2022b), including V, Rb, Sr, Zr, Nb, Ba and Th. Barium is significant because of the presence of abundant baryte (Ixer et al., 2019; Bevins et al., 2020) together with calcite as a cement in the Altar Stone. However, Ca concentrations, along with other light (low atomic number) elements, are affected by moisture in pXRF analysis and by surface features/alteration, so are not considered here. In addition, Bevins et al. (2022a) and Bevins et al. (2023) noted that Ca had been leached from some of the *in situ* Altar Stone analyses.

As noted above, the Altar Stone contains high Ba, with all but 1 of the 106 analyses (plotted in red on Figs. 2 and 3) containing > 1025 ppm, the outlying analysis coming from Area C of the Altar Stone (Bevins et al., 2022a) which was difficult to access, being partly under Stone 156 (a fallen lintel) and partly under Stone 55b (part of the Great Trilithon). Barium concentrations are clearly far higher in the Altar Stone than the majority of Anglo-Welsh Basin (AWB) ORS samples, with only four AWB ORS samples having analyses which exceed 1000 ppm: these samples – WM 6, 2009.46G.R.3a, LSF2-5504 and LORS 27 (locations shown on Figure 1) – are plotted with black symbols in Figs. 2 and 3. The remaining 54 AWB ORS samples are not individually identified in Figs. 2 and 3 and are plotted as green triangles. Strontium concentrations are also generally higher in the Altar Stone (104 analyses > 86 ppm) than the AWB ORS samples, although a few AWB ORS analyses exceed 300 ppm Sr (not shown on Fig. 2 but see Supplementary Table 2). The Ba-Sr distribution clearly separates the Altar Stone from the majority of AWB ORS samples, with a strong positive correlation between Ba and Sr in the Altar Stone ($Sr = 0.0092 Ba + 91$, $r = 0.71$), whereas the relationship between all AWB ORS samples is poor ($r = 0.15$). Of the four high-Ba (>1000 ppm) ORS samples, WM 6 has a similar Ba-Sr composition to the Altar Stone, the two high Ba analyses in LSF2-5504 have higher Sr than the Altar Stone, 2009.46G.R.3a has $Sr < 86$ ppm in its four high-Ba analyses, as does the sole high-Ba analysis from LORS 27, although these samples both sit in the extended envelope of all Altar Stone analyses. We take the strong Ba-Sr correlation to reflect that Sr in the Altar Stone substitutes for Ba in the baryte.

However, the Ba-Rb plot shows that 2009.46G.R.3a, LORS 27 and LSF2-5504 all have Rb contents a factor of ~ 3 higher than in the Altar Stone, ruling out a possible relationship. A similar relationship is seen with K (not plotted). WM 6, however, has similar Rb concentrations to the Altar Stone. Zirconium concentrations overlap for the Altar Stone and AWB ORS samples; however, many AWB ORS samples have Zr contents much lower than the Altar Stone, and a few Altar Stone analyses exceed the AWB ORS concentrations. In terms of Zr and Nb, there is an overlap of WM 6 and 2009.46G.R.3a with the Altar Stone analyses, but for the Altar Stone $Nb = 0.0126 Zr + 7.35$ ($r = 0.91$), whilst for the AWB ORS samples $Nb = 0.0194 Zr + 5.2$ ($r = 0.58$), possibly indicative of source regions with different Zr/Nb ratios.

For the ORS samples, $V = 3.56 Nb + 54$ ($r = 0.15$), but for the Altar Stone $V = 1.38 Nb + 32.5$ ($r = 0.34$). Both V and Nb are likely to be associated with Fe-Ti and Ti oxide (probably rutile) phases where Nb will likely substitute for Ti, and V for Fe (GERM, 2021; Rollinson and Pease, 2021), V particularly favouring inclusion within magnetite. Here, WM 6 does not plot with the Altar Stone analyses, having higher V,

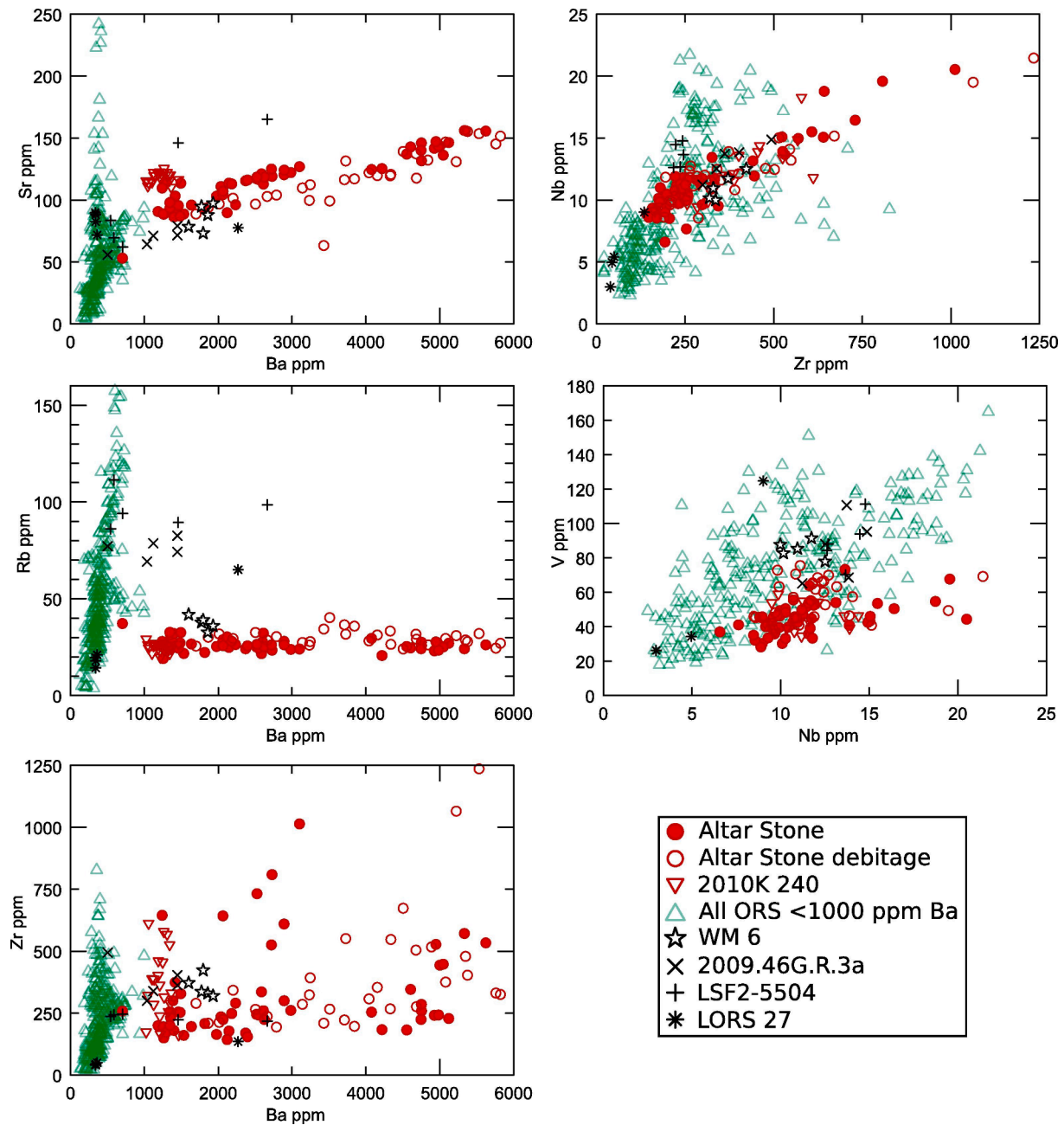


Fig. 2. Bivariate plots of geochemical data for the Altar Stone and its related samples (red symbols), and undifferentiated Old Red Sandstone samples analysed in the study plotted in green with those samples containing > 1000 ppm Ba labelled separately (black symbols). On these diagrams, despite four samples containing more than > 1000 ppm Ba, only WM 6 plots consistently close to the field of data from the Altar Stone. The plot of Nb - V excludes all analyses from WHB-3 (see [Supplementary Table 1](#)) which has V between 240 and 410 ppm.

which may separate it from the Altar Stone. This difference is consistent with the high concentration of altered titaniferous magnetite (now martite) and titaniferous hematite in WM 6 and their total absence in the Altar Stone. The different V/Nb ratios between the ORS samples and the Altar Stone may suggest a different mix of, or source for, the Fe-Ti oxides, also consistent with the mineralogy of the opaque phases. Slightly more overlap is shown for Nb and Ti (not plotted) which shows WM 6 with concentrations similar to the highest in the Altar Stone, but the AWB ORS samples again have generally higher Ti.

Fig. 3 presents three triangular diagrams which confirm some of the associations described above. The clearest distinction between the ORS and the Altar Stone samples is seen in the alkali and alkaline earth metals Ba, Sr and Rb, with only WM 6 showing any similarity to the Altar

Stone. The highly incompatible and immobile elements Zr, Nb, and Th, which will reside in accessory phases in the sandstones, show a general overlap, suggestive of generally similar sources and processes. The Ti-V-Nb plot, however, suggests that the Altar Stone has lower Ti and V, and higher Nb than the AWB ORS samples, possibly related to Fe-Ti and Ti oxides, with WM 6 plotting in the middle of the ORS field, and slightly offset from the Altar Stone compositions.

From the above it is clear that the majority of the AWB ORS samples have a very different chemical composition from the Altar Stone, with only four ORS samples showing Ba > 1000 ppm. Of these four high-Ba samples, WM 6 is the only one which consistently plots close to, but not always within, the field of compositions of the Altar Stone. We have investigated these four samples further using automated SEM-EDS and

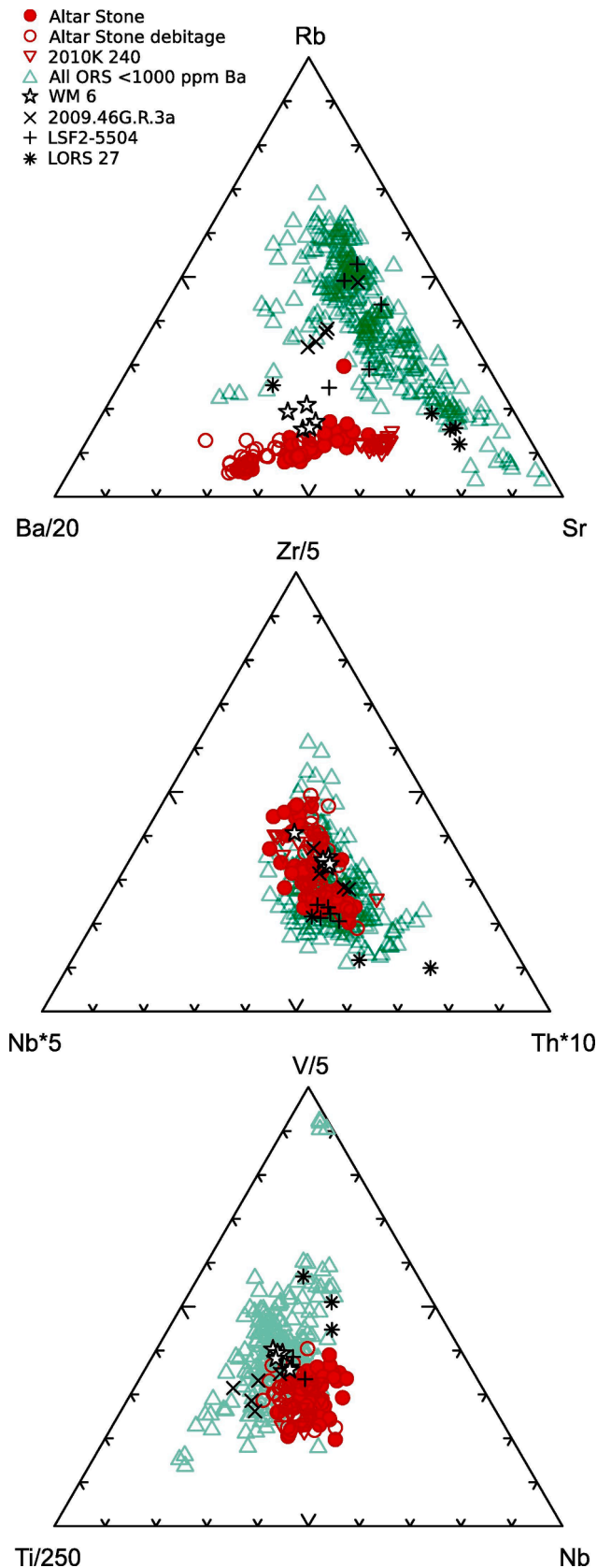


Fig. 3. Triangular variation diagrams for the alkali/alkali earth metals Ba-Sr-Rb, the highly incompatible elements Nb-Zr-Th, and elements associated with Fe-Ti oxides, viz. Ti-V-Nb.

preliminary Raman Spectroscopy (for WM 6), as detailed below, comparing with data from the Altar Stone and derived fragments, and finally make comparisons with our findings based on standard petrography.

4. Automated SEM-EDS

Earlier work has utilised automated SEM-EDS analysis to quantify the mineralogy in a textural context of the Altar Stone along with other bluestone lithologies (Ixer et al., 2019; Ixer et al., 2022; Ixer et al., 2023; Bevins et al., 2020; Bevins et al., 2021; Bevins et al., 2022a; Bevins et al., 2023) and samples from one of the sarsen stones (Nash et al., 2021). Based on the pXRF geochemical analyses, the four ORS samples with Ba compositions comparable to the Altar Stone were selected for detailed mineralogical analysis.

4.1. Analytical methods

Previous analyses utilised a QEMSCAN automated SEM-EDS platform; however, in this study the analysis was carried out using an AMICS system. Analysis was undertaken using a Hitachi SU3900 scanning electron microscope fitted with two large area (60 mm²) Bruker SDD energy dispersive spectrometers and running the Bruker AMICS automated mineralogy package. Beam conditions were optimised for analysis and therefore an accelerating voltage of 20 kV coupled with a beam current of approximately 10nA was used. All samples were measured using the same analytical parameters and, to retain consistency with previous (QEMSCAN) analyses, a mapping mode of analysis was used. This analytical mode first acquires a high-quality BSE image and then systematically steps the electron beam across the sample at a preset stepping interval of, in this case, 10 μm. An EDS X-ray spectrum is collected at each point, compared with a spectral library of known minerals and compositions, and a mineral assignment is made.

4.2. Comparison of results from the AMICS and QEMSCAN platforms

All automated SEM-EDS systems are based on the same technology, but the data processing software differs. To allow direct comparison between the previous analyses carried out using a QEMSCAN platform, the new AMICS-based analyses replicated the previously reported mineral groupings. To test the comparison between the different analytical platforms we repeated the analysis of two samples (2010 K 240 and WM 6) using AMICS, which had previously also been analysed using the QEMSCAN platform. These replicate analyses used the same polished thin sections, although the exact area of the sandstone measured in the analyses will have differed slightly and hence some sample variance can be expected. The replicate analyses for the two samples are provided in Table 1 and are shown graphically in Fig. 4. Based on the data presented in Table 1 and Fig. 4 there is a very strong correspondence between the replicate analyses. Key, albeit small, analytical differences are that reported muscovite abundance is higher within the QEMSCAN analyses rather than the AMICS data (2.32 / 2.82 % versus 1.05 / 1.28 % respectively); it is likely that some areas reported as muscovite in the QEMSCAN analysis are reported to the illite mineral categories in the AMICS dataset and vice versa. Dolomite is also apparently more abundant in the QEMSCAN dataset when compared with the AMICS data; the apparent increase in the calcite abundance in the AMICS data suggests that dolomite is reporting to the calcite mineral grouping or vice versa. All other mineral categories are within expected variance for replicate analyses (see Pirrie et al., 2009). Neither dolomite nor muscovite abundance is a critical characteristic discriminator in terms of comparison between known Altar Stone and questioned ORS samples. It is reasonable, therefore, to make comparisons between the new AMICS-generated results with those from previous QEMSCAN-generated results.

Table 1

Comparison of replicate analyses using both a QEMSCAN and an AMICS automated SEM-EDS mineralogy platform.

Analytical System	2010 K 240a		2010 K 240b	
	QEMSCAN	AMICS	QEMSCAN	AMICS
Quartz	51.03	52.69	53.83	54.73
K Feldspar	0.34	0.25	1.27	1.23
Plagioclase	12.15	11.59	10.45	10.71
Muscovite	2.32	1.05	2.82	1.28
Biotite	0.48	0.48	0.83	0.85
Kaolinite	3.37	3.18	2.63	3.14
Chlorite	4.05	3.59	6.51	4.37
Illite & Illite-smectite	4.97	5.14	6.42	6.51
Fe-Illite & Illite-smectite	0.89	1.59	4.51	4.97
Calcite	18.80	19.44	9.10	10.29
Dolomite	0.59	0.01	0.20	0.01
Ferroan Dolomite	0.04	0.00	0.03	0.00
Fe Oxides	0.00	0.00	0.32	0.44
Chromite	0.01	0.02	0.02	0.02
Pyrite	0.00	0.00	0.00	0.00
Baryte	0.13	0.11	0.27	0.24
Anhydrite	0.00	0.00	0.00	0.00
Halite	0.00	0.00	0.00	0.00
Rutile & Ti Silicates	0.37	0.31	0.27	0.23
Ilmenite	0.04	0.08	0.19	0.19
Apatite	0.24	0.20	0.16	0.16
Garnet	0.05	0.09	0.13	0.48
Tourmaline	0.06	0.03	0.02	0.03
Zircon	0.05	0.05	0.03	0.05
Undifferentiated	0.00	0.09	0.00	0.07

4.3. New results

The mineralogical data for samples 2009.46G.R.3a, LORS 27, LSF2-5504 and WM 6 are provided in Table 2 and are plotted in Fig. 5 against previous analyses of samples proven as derived from the Altar Stone. Based on the overall modal mineralogy there are significant mineralogical differences between the analyses of samples confirmed as derived from the Altar Stone and the four ORS samples selected for analysis. The mineralogical data support the pXRF data which indicate that if samples 2009.46G.R.3a, LORS 27 and LSF2-5504 are representative of the location sampled, then these localities can be excluded as the source of the Altar Stone. Geochemically sample WM 6 is the only one which consistently plots close to the field of compositions of the Altar Stone but the automated mineralogy data show that it differs mineralogically based on the abundance of detrital K feldspar, plagioclase and Fe oxides and diagenetic calcite and baryte (which are key characteristics of the Altar Stone mineralogy). Consequently, based on the automated mineralogy dataset, if sample WM 6 is representative of the location from which it was collected, then this area too can be excluded as the source area for the Altar Stone.

5. Raman Spectroscopy

Raman Spectroscopy in provenance studies can be used both as a mineralogical fingerprint and also to allow inferences to be made as to the geological and geographical sources of sediment (Garzanti and Andò, 2007a). This is widely applied to both modern, unconsolidated sandy/silty sediments (Andò et al., 2011) as well as sedimentary rocks (Garzanti and Andò, 2007b). Here we have applied Raman Spectroscopy to compare the Anglo-Welsh Basin ORS sample WM 6 (see above) to MS-1, one of the debitage fragments derived from the Altar Stone (Iser et al., 2019; Bevins et al., 2020; Bevins et al., 2022a), to assess whether their chemical similarity reported above is reflected in their mineralogy and how this mineralogy compares with that determined by automated SEM-EDS.

The technique can be undertaken with mineral grain sizes down to a

few microns, is non-destructive, and can be applied to minute quantities of material. As well as providing mineral abundance data, mineral compositional information is also generated, and this method has applications in geoarchaeological studies (Zimmermann et al., 2016).

5.1. Sample preparation and analysis methods

Small amounts from the two samples analysed were first disaggregated and then the heavy minerals (HMs) were concentrated following the protocol for gravimetric separation developed by Andò (2020) in order to calculate the heavy mineral abundance in the two samples. A Renishaw inVia Reflex® Raman Spectrograph at the Università di Milano-Bicocca was used with a 50x long working distance (LWD) objective, coupled to a green laser ($\lambda = 532$ nm). Raman spectra were collected in the 150–1200 cm^{-1} spectral range and in the high frequency OH^- region around 3100–4000 cm^{-1} for hydrated minerals, this combination allowing identification of individual mineral types as well as mineral varieties. The masses available for the two samples required different methods of preparation, as described below. Optical analysis, in transmitted and reflected light using a polarizing microscope (Mange and Maurer, 1992), was combined with a single grain Raman Spectroscopy approach (Andò et al., 2011; Andò and Garzanti, 2013) in order to quantify mineral abundances in the heavy mineral separates.

5.1.1. MS-1 – Altar Stone debitage fragment

Only 0.1973 g of sample MS-1 (>2 μm) was available for study, being the residue following X-ray diffraction (XRD) analysis of a detached fragment from the sample. This is close to the limit of the gravimetric protocol for heavy mineral separation using only a few milligrams available in forensic investigations. After wet sieving at 500 μm using a steel sieve, the sample was dried and weighed, with the >500 μm fraction giving 0.0231 g and the >2 –500 μm fraction giving 0.1453 g (74 % of the sample). The sieved yield represented a weight loss of ~ 15 %, considered acceptable when working with samples of only fractions of a gramme. The 2–500 μm fraction was separated into heavy and light mineral fractions in a centrifuge using the non-toxic heavy liquid sodium polytungstate (SPT) at a density of 2.90 g/cm^3 . The light fraction weighed 0.1334 g and the total heavy mineral grains were 0.002 g, representing only 1.4 % by weight of the sample, 2 mg being the minimum amount of material for preparing a grain mount.

For MS-1 all the separated heavy mineral grains were mounted on a slide with Canada Balsam ($n = 1.54$) for optical identification of the mineralogy, to document the texture of single grains and to perform analyses by Raman Spectroscopy. Considering the wide grain size range this HM sample comprises (2–500 μm), it is essential to apply a point counting method to determine the mineral frequency which can then be transformed into abundance percentages by accounting for the grain volumes. Observations in transmitted and reflected light enable the entire mineral population to be described, here giving 206 transparent HM grains and 325 opaque, turbid, phyllosilicate, carbonate and “light minerals”. Raman Spectroscopy is then finally applied to the mineral separate to differentiate magmatic (schorl) versus metamorphic (dravite) tourmalines, garnet types, apatite, and carbonates. In MS-1, HM grains are well sorted, mostly sub-rounded, with very rare opaque minerals, no Fe-hydroxides, and Ti-oxides comprising 12 % of semi-opaque heavy grains (Fig. 6). In the transparent HM suite, apatite (29 %) is dominant, occurring with zircon (9 %), garnet (8 %), rutile (6 %), tourmaline (4 %), red spinel (2 %), with trace quantities of blue-green amphibole, anatase and epidote. Baryte is very common (40 %), occurring with “light minerals” (27 %), chlorite (15 %), authigenic Ti-oxides (12 %) (occurring as granular rutile and anatase), undifferentiated carbonates (5 %, not calcite), and biotite (2 %). Apatite shows a well-rounded to sub-rounded shape, whilst baryte is more angular with corroded rims, and chlorite is larger in size and rounded to sub-rounded.

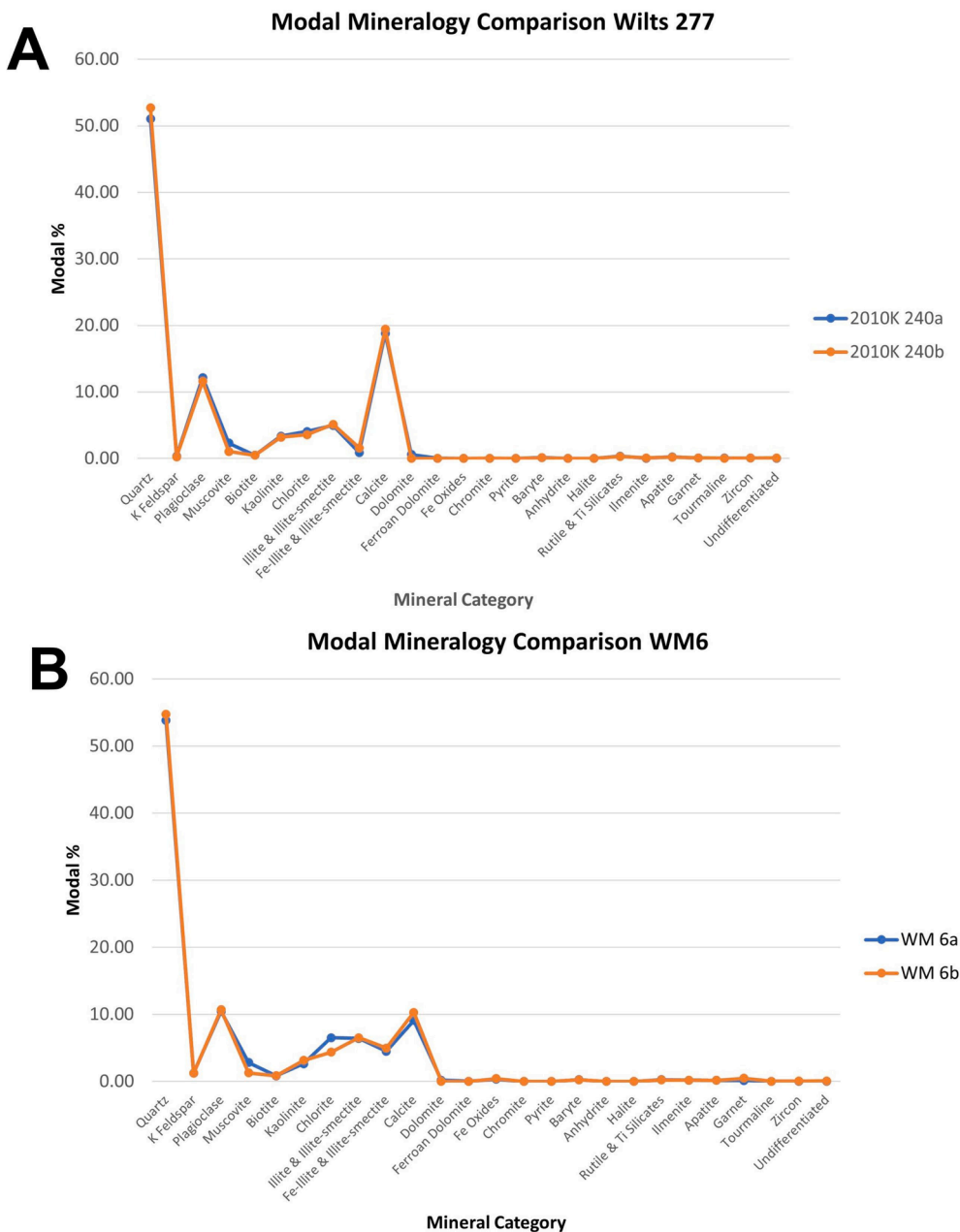


Fig. 4. Comparison of the reported modal mineralogy for samples (A) 2010 K 240 and (B) WM 6 based on replicate analyses using both QEMSCAN (analysis a) and AMICS (analysis b) automated SEM-EDS platforms.

5.1.2. WM 6: Anglo-Welsh Basin ORS sample from the West Midlands

A larger sample of WM 6 was available for analysis, which had been previously disaggregated for XRD analysis. The quantity of powder was sufficient to apply a standard preparation protocol, and a representative aliquot was obtained by splitting it using the method of Parfenoff et al. (1970) to give an initial dried fraction of 2.0515 g.

After wet sieving the sample at 500 µm with a steel sieve, the > 500 µm fraction was 0.0047 g, the 5–500 µm fraction was 1.8553 g (90 % of the sediment), with 0.1406 g < 5 µm. The 5–500 µm fraction was centrifuged in SPT, giving a light fraction of 1.7694 g and the heavy grains of 0.0393 g (2.1 % by weight). A representative aliquot of HMs was obtained using a micro-riffle box and prepared as a grain mount with Canada Balsam. Once again, considering the wide grain size range (5–500 µm), a heavy-mineral point counting method was applied. Optical inspection identified 200 transparent HMs together with 372 opaque, turbid grains, phyllosilicates, carbonates and “light minerals”.

Heavy mineral grains in WM 6 are poorly sorted, most of the grains are angular, and both opaque minerals (16 %) and semi-opaque Fe-hydroxides are common (15%). In the transparent HM suite, garnets (28 %) are dominant, occurring with apatite (13 %), zircon (11 %), rutile and spinel (3 %), tourmaline (2%), and trace amounts of epidote and anatase (1 %). Other common minerals in WM 6 include Ti-oxides (13%), the platy minerals chlorite (9%) and biotite (5%), mostly deeply weathered), and finally “light minerals” (5%) and minor carbonate (1%, not calcite).

5.1.3. Comparison between WM6 and Altar Stone samples

The HM compositions of MS-1 (Altar Stone) and WM 6 (ORS) are compiled in Table 3. Raman analyses of detrital HM suites show markedly different HM abundances for the two analysed samples, indicating they are different from each other and from different sources. Specifically, the Altar Stone contains well sorted HMs, which are mostly sub-

Table 2

Modal mineralogy of selected ORS samples with elevated Ba geochemical signatures based on AMICS analysis.

	WM 6	LORS 27	LSF2.5504	2009.46G.T.3
Quartz	54.73	50.76	48.70	57.35
K Feldspar	1.23	3.44	0.06	0.02
Plagioclase	10.71	0.06	14.10	16.15
Muscovite	1.28	0.73	2.36	2.63
Biotite	0.85	0.25	1.41	2.79
Kaolinite	3.14	0.20	0.06	0.06
Chlorite	4.37	1.30	4.24	6.08
Illite & Illite-smectite	6.51	3.01	11.58	8.29
Fe-Illite & Illite-smectite	4.97	0.98	3.60	4.12
Calcite	10.29	38.73	13.23	1.23
Dolomite	0.01	0.35	0.00	0.00
Ferroan Dolomite	0.00	0.03	0.00	0.00
Fe Oxides	0.44	0.03	0.00	0.06
Chromite	0.02	0.00	0.01	0.02
Pyrite	0.00	0.00	0.00	0.00
Baryte	0.24	0.00	0.11	0.10
Anhydrite	0.00	0.00	0.00	0.00
Halite	0.00	0.00	0.00	0.00
Rutile & Ti Silicates	0.23	0.05	0.34	0.48
Ilmenite	0.19	0.01	0.01	0.00
Apatite	0.16	0.03	0.01	0.15
Garnet	0.48	0.03	0.06	0.13
Tourmaline	0.03	0.01	0.02	0.03
Zircon	0.05	0.00	0.04	0.06
Undifferentiated	0.07	0.00	0.05	0.25

rounded, with very rare opaque minerals and no Fe-hydroxides, as well as containing 29% apatite, 8% garnet (mainly solid solutions of almandine and spessartine) and 4% tourmaline (both schorl and dravite). In contrast WM 6 contains HMs which are poorly sorted and angular, with only 13% apatite, and both opaque minerals (16%) and semi-opaque Fe-hydroxides being common (15%), whilst garnet is abundant (28%) but apatite (13%) and tourmaline (1.5%) less so (dravite being absent). These differences clearly indicate that WM 6 and

MS-1 were not sourced from the same lithologies and hence have different sources.

6. Comparisons between results of standard petrographic examinations of WM 6 and the Altar Stone and results from automated SEM-EDS and Raman Spectroscopy

Standard petrographic examination generally concurs with the automated SEM-EDS and Raman Spectroscopy results but does provide additional information. There are some differences of note between the standard petrography results and the analytical investigations of sample WM 6 and samples proven to have been derived from the Altar Stone. In thin section, whilst the detrital grains in WM 6 are dominated by monocrystalline straight extinction quartz, along with plagioclase and K feldspar, there are also abundant mudstone clasts (Fig. 7), the latter not seen in the analytical investigations. These mudstone clasts are typically compacted and commonly form a pseudo-matrix around the quartz grains. These grains could potentially either be mudstone lithic sedimentary clasts, or alternatively, mudstone intraclasts. Kaolinite, chlorite, illite and Fe-illite are reported as present in both the known Altar Stone samples, in this case 2010 K 240, in which the total clay content is 13.5% (AMICS data), and also in WM 6, but the total clay content is significantly higher (19%; again AMICS data) in the latter section. In addition, sample WM 6 is notably coarser grained than 2010 K 240, as illustrated in Fig. 7.

Altar Stone sample 2010 K 240 and ORS sample WM 6 have sharply contrasting opaque mineralogies, most clearly evidenced by the occurrence of hematite. It is notably present in WM 6 (0.44%; AMICS data) as martite replacing primary magnetite but also within ilmenohematite and as titaniferous hematite-rutile intergrowths; much occurs as fine-grained intergrowths with TiO₂ minerals replacing original iron titanium oxides including ilmenite. Hematite pigment (<1 μm size crystals) is also widespread within the matrix and occurs along the cleavage planes of altered biotite. This contrasts with the almost total absence of hematite in the Altar Stone (AMICS analyses show 0.00% Fe oxides),

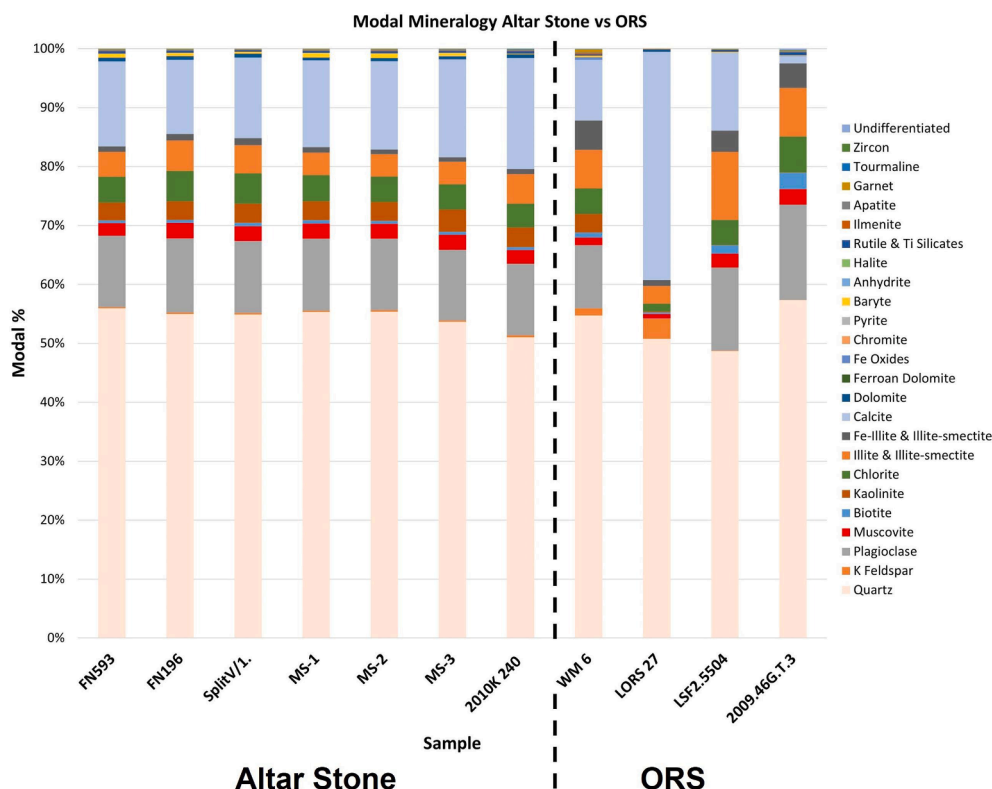


Fig. 5. Modal mineralogy of samples confirmed as derived from the Altar Stone compared with the analysed ORS samples.

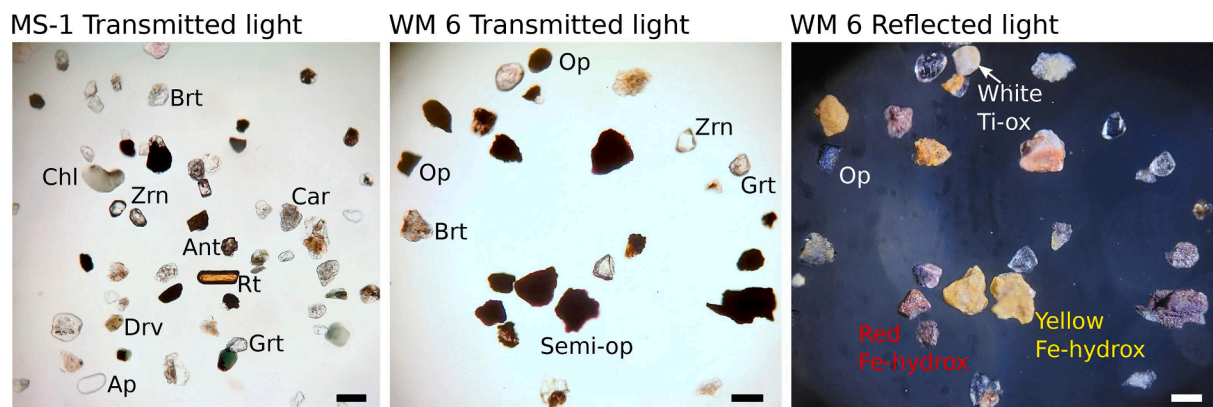


Fig. 6. Heavy mineral grain mounts (mounting medium $n = 1.54$) displaying different heavy-mineral suites. MS-1 is dominated by transparent heavy minerals, with common sub-rounded grains compared with WM 6 which shows abundant, larger, angular semi-opaque Fe-oxides and hydroxides with a different suite of HMs dominated by corroded and etched garnets. Abbreviations (alphabetic order) follow [Kretz \(1983\)](#): Ant - Anatase; Ap - Apatite; Brt - Baryte; Car - Carbonate (unspecified); Chl - Chlorite; Fe-Hydrox - Red and yellow-orange Fe-hydroxides; Grt - Garnet; Op - Opaque (unspecified); Rt - Rutile; Ti-Ox - White Ti-oxides; Zrn - Zircon. Scale bar = 100 μm .

Table 3

Frequency of heavy mineral grains in samples MS-1 and WM 6 from Raman Spectroscopy analysis. Numerical grain frequency counted by optical microscopy in transmitted and reflected light using a point counting method (PCm). Percentages of grain size fractions and of total heavy grains (%HM/Tot) included here. Percentage grain frequency recalculated from numerical count data. Zircon-Tourmaline-Rutile (ZTR) index after [Hubert \(1962\)](#). Percentage of total heavy grains (%HM/Tot) and percentage of transparent heavy minerals in weight (tHM %weight) given, with varieties of tourmaline (schorl or dravite) indicated.

Numerical grain frequency			Percentage Grain Frequency		
Location	Stonehenge	West Midlands	Location	Stonehenge	West Midlands
Sample	Altar Stone	ORS	Sample	Altar Stone	ORS
Number	MS-1	WM 6	Number	MS-1	WM 6
Class analysed	2-500 μm	5-500 μm	HM tot%	1.4	2.1
Counting method	PCm	PCm	tHM %weight	0.5	0.7
Operator	Sergio Ando	Sergio Ando	zircon	8.7	11.0
zircon	18	22	tourmaline	3.9	1.5
dravite	2	0	rutile	6.3	3.0
schorl	6	3	Ti Oxides	1.0	1.0
rutile	13	6	apatite	29.1	13.0
anatase	2	2	others	39.8	39.0
apatite	60	26	epidote	0.5	1.0
baryte	82	78	garnet	7.8	27.5
blue-green hornblende	2	0	amphibole	1.0	0.0
spinel	4	6	spinel	1.9	3.0
epidote	1	1	Total	100 %	100 %
clinozoisite	0	1	ZTR	19	16
garnet	16	55	% transparent HM	39 %	35 %
Total transparent	206	200	% opaque HM	0 %	16 %
opaques	2	94	% Fe Ox	0 %	15 %
Fe Ox-Hydrox	0	87	% Ti Ox	12 %	13 %
Ti Ox	65	77	% chlorite	15 %	9 %
chlorite	79	52	% biotite	2 %	5 %
biotite	10	28	% carbonates	5 %	1 %
carbonates	28	6	% "light minerals"	27 %	5 %
"light minerals"	141	28	Total	100 %	100 %
Total Opaque	325	372	zircon	8.7	11.0
Total (all)	531	572	dravite	1.0	0.0
<5 μm (g)	0.000	0.141	schorl	2.9	1.5
5-500 μm (g)	0.145	1.855	rutile	6.3	3.0
>500 μm (g)	0.023	0.005	anatase	1.0	1.0
% fine tail cut (g)	0 %	7 %	apatite	29.1	13.0
% class (g)	74 %	90 %	baryte	39.8	39.0
% coarse tail cut (g)	12 %	0 %	blue-green hornblende	1.0	0.0
TOT excluded (g)	12 %	7 %	spinel	1.9	3.0
Total sieved (g)	0.1973	2.0515	epidote	0.5	0.5
Total used (g)	0.145	1.855	clinozoisite	0.0	0.5
Light fraction (g)	0.133	1.769	garnet	7.8	27.5
Dense fraction (g)	0.002	0.039	Total Transparent	100 %	100 %
%HM/Tot	1.4	2.1			

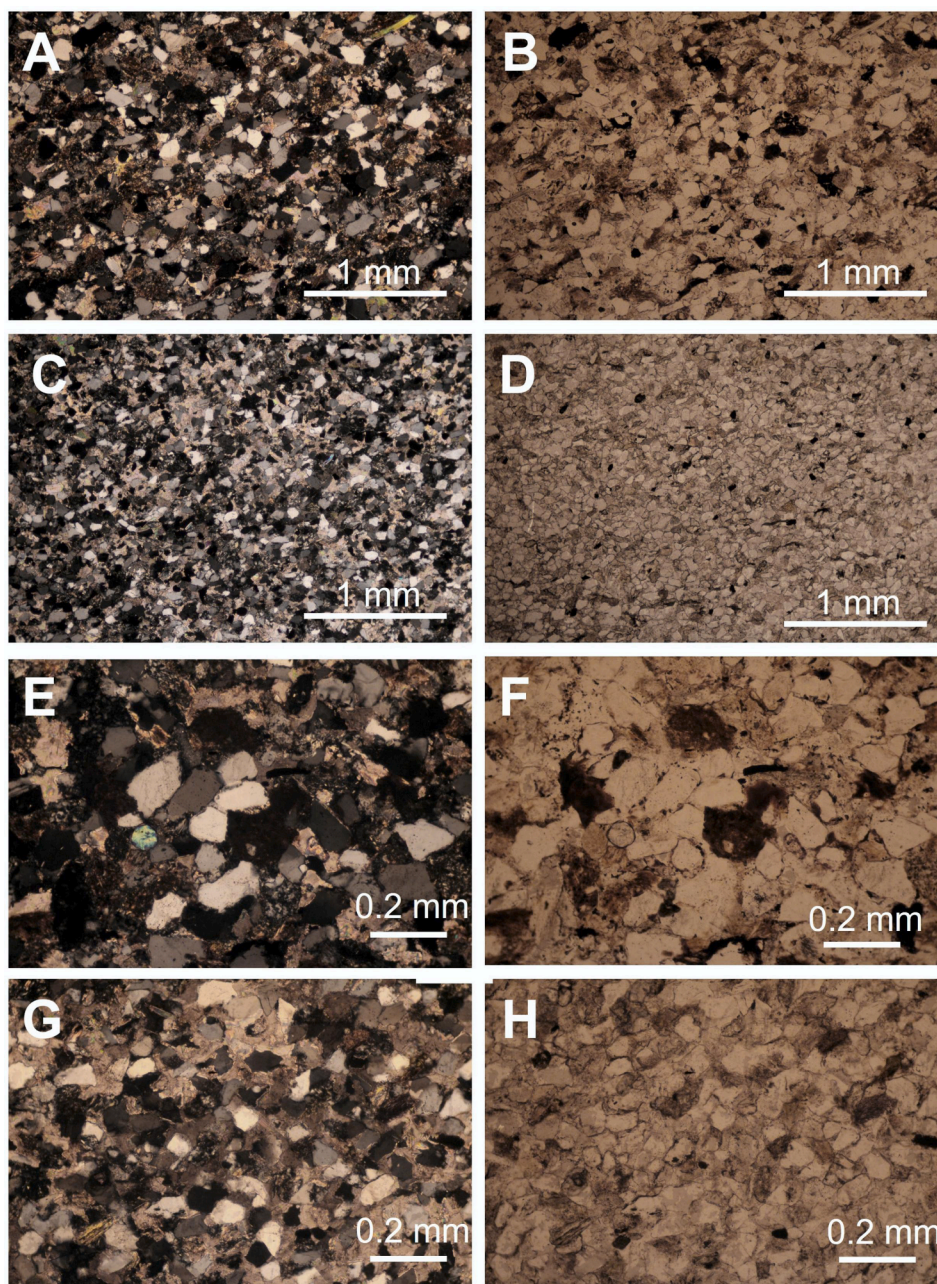


Fig. 7. Petrographic comparison of Sample WM 6 (A, B, E, F) with sample 2010 K 240 (C, D, G, H), which is proven to be derived from the Altar Stone. Images A, C, E, G cross polarised light; B, D, F, H plane polarised light. Note the abundance of mudstone clasts in WM 6 when compared with 2010 K 240.

where primary iron titanium oxides only comprise fine-grained secondary TiO_2 minerals (their original secondary fine-grained hematite being lost). This is reflected at the hand specimen/outcrop scale, WM 6 being a red sandstone whilst the Altar Stone is grey-green.

7. Discussion - where next?

Based on the pXRF sample screening and more detailed integrated geochemistry and mineralogy all of the examined locations from the Old Red Sandstone in the Anglo-Welsh Basin can be excluded as the source of the Altar Stone. No other ORS locations with comparable Ba concentrations as observed in the Altar Stone are known in outcrops of the Anglo-Welsh Basin, thus suggesting that we should perhaps exclude the Anglo-Welsh Basin from further investigations, leading us to consider broadening our horizons, both geographically and stratigraphically.

Key sedimentological characteristics of the Altar Stone are that it is a

very fine- to fine-grained, well sorted sandstone. Unidirectional ripple cross lamination is present and is defined by the presence of subtle heavy mineral laminae. At the thin section scale there is no apparent bioturbation and no fossils are recognised within the samples examined. The sandstone has undergone moderate compaction, with the calcite cement inferred to relate to burial diagenesis. However, there is no apparent tectonic fabric (e.g. cleavage) implying that it has not undergone significant deformation. In addition, there is also a lack of stylolites or chemical dissolution surfaces which might result from such deformation.

The overall dimensions of the Altar Stone at Stonehenge and its geometry (measuring 4.9 m long by 1 m wide by 0.5 m thick) suggest that the original bed thickness must be > 50 cm, with widely spaced (~ 5 m) vertical joint sets; the tabular nature suggests that the original bed geometry has a tabular rather than strongly channelised or lenticular form. Clearly, unidirectional ripple cross lamination can develop in a very

wide range of depositional settings, although the presence of the heavy mineral laminae would be more consistent with a fluvial depositional system. The absence of trace or body fossils may also indicate that a non-marine depositional setting is perhaps more likely. Overall, the sediment characteristics and lack of evidence for tectonism or significant metamorphism would suggest that the source of the Altar Stone was a post Caledonian, non-marine Devonian or post-Devonian sandstone unaffected by tectonism.

The detrital mineralogy of the Altar Stone is dominated by sub-angular to sub-rounded monocrystalline quartz grains showing

straight extinction although rare, larger grains are strained. Plagioclase is much more abundant than K feldspar. Lithic grains (rock fragments) are the same size as the quartz and feldspar grains; most are internally fine-grained and include siliceous “cherts”, polycrystalline metamorphic quartz, phyllite and fine-grained sandstone, along with rare, fine-grained graphic granite and quartz-chlorite intergrowths. Detrital muscovite dominates over biotite. Heavy minerals identified optically and through automated mineralogy and Raman Spectroscopy include Fe oxides, chromite, rutile and Ti oxides, rare ilmenite, apatite, garnet (mostly almandine and spessartine), tourmaline (mostly schorl) and

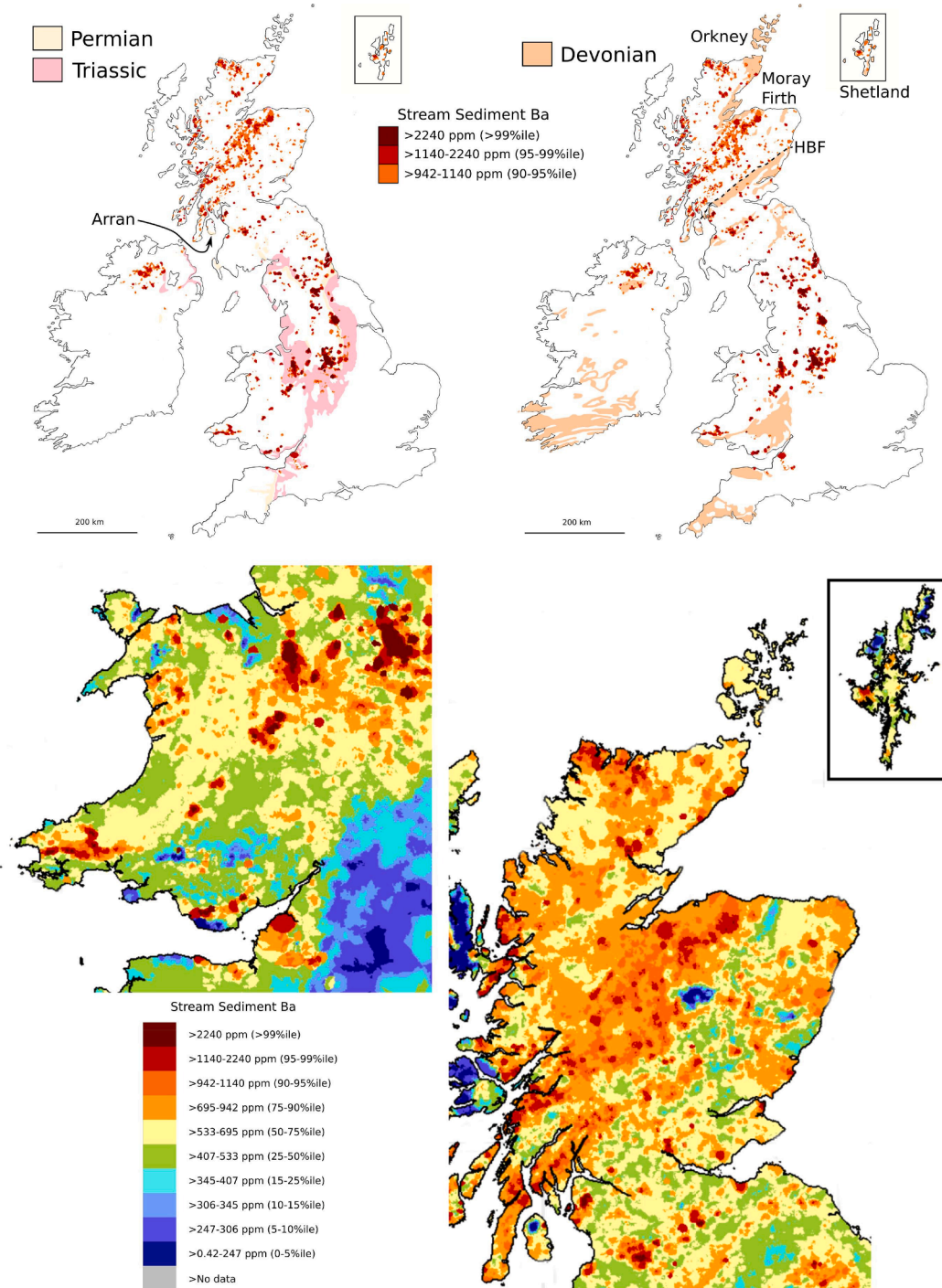


Fig. 8. Outline geological maps contain British Geological Survey materials © UKRI [2023] from BGS Make-a-Map (<https://www2.bgs.ac.uk/discoveringgeology/geology-of-britain/make-a-map/map.html>). Stream sediment geochemistry data from the G-Base project, contains British Geological Survey materials © UKRI [2023] from <https://www.bgs.ac.uk/datasets/g-base-for-the-uk/>.

zircon.

Geochemically, the Altar Stone is characterized principally by its high Ba content, related to the presence of a baryte cement, with an average Ba abundance of around 2800 ppm. This contrasts markedly with the average of all of the ORS samples analysed from the Anglo-Welsh Basin, with Ba averaging 437 ± 293 ppm (range 128–2665 ppm). Baryte is a highly insoluble mineral, resistant to chemical weathering, and for this reason Ba concentrations in stream sediments often closely reflect the underlying geology (British Geological Survey, 2000; Everett et al., 2019). In the stream sediments lying on the ORS in Wales, Ba concentrations are typically between the 5th–75th percentile of the national range (Everett et al., 2019), being between 247 and 695 ppm, which compares well with the pXRF analyses (average 437 ± 293 ppm, see Fig. 8). It is to be expected therefore that the strata which sourced the Altar Stone would have elevated Ba. Fig. 8 shows simplified geological maps for the UK which indicate the outcrop of Devonian and Permo-Triassic rocks, these being predominantly non-marine strata which are geologically consistent with the lithology of the Altar Stone. These maps are superimposed on geochemical maps highlighting areas where Ba in stream sediments exceeds 942 ppm (>90th percentile), which may provide clues as to the source of the Altar Stone. Also shown in Fig. 8 are sections of the detailed Ba stream sediments maps, which at a larger scale show some of the high-Ba regions more clearly. The lack of high Ba over Devonian sequences in Wales is clear, although there is high Ba on the north Somerset coast, but these are deformed Middle Devonian marine sequences and thus could not be the source of the Altar Stone. There is elevated Ba in Northern Ireland (no Ba stream sediment data exists for the Republic of Ireland) over dominantly conglomeratic Middle Devonian sediments. In NE Wales, Cheshire and the Welsh Borderland, high Ba coincides with Permo-Triassic sequences, as does local Pb-Zn-baryte mineralisation. Perhaps of significance is the fact that there is just a single significant Neolithic monument in the NE Wales/Cheshire/Merseyside area, that being the remains of a megalithic tomb comprising six red sandstone orthostats with carved motifs known as the Calderstones in Allerton near Liverpool (Forde-Johnston, 1958). Interestingly, in this area during the Bronze Age, Alderley Edge was the site of one of the earliest known copper mines in Britain in baryte-bearing, sometimes pebbly, Triassic sediments. High Ba is recorded between Leeds and York, while on the eastern edge of the Triassic sequences adjacent to the Pennine Fault there is high Ba, the latter associated with mineralisation in the Pennine ore field (Colvine, 1995). Here, however, no significant Neolithic monuments occur in these areas, although further north in the Vale of Eden area a string of monuments occurs, including the stone circle known as Long Meg and her Daughters (Sharpe, 2022). Long Meg itself is a 3.8 m monolith consisting of red sandstone, generally thought to have been cut from cliffs of the Permian Penrith Sandstone Formation bordering the River Eden close by.

Further north, in Scotland, non-marine Old Red Sandstones are more abundant than Permo-Triassic sequences. On the east and west coasts of the Isle of Arran, stream sediment Ba exceeds 942 ppm, associated with Permian or ORS sequences (British Geological Survey, 1993). On the west coast of Arran there are remains of a number of Neolithic stone circles at Machrie Moor. Circles 2 and 3 are of pebbly red sandstone, probably Permian in age and thought to be from nearby Auchagallon (see Richards, 2013). Another high-Ba occurrence is above similar Permian lithologies east of Prestwick, and there are a small number of high-Ba locations above ORS strata in the Midland Valley (south of the Highland Boundary Fault), but once again these are not associated with known Neolithic contexts. What is interesting to note is that Hillier et al. (2006) reported the presence of a dioctahedral interlayered chlorite-smectite (tosudite) in sandstones of the ORS Strathmore Group in the Midland Valley Basin. Tosudite also occurs in the Altar Stone sandstone (authors' unpublished data). North of the Highland Boundary Fault, ORS strata occur in the Orcadian Basin, around the Moray Firth, through Sutherland, and on Orkney and Shetland. Across these sandstone areas

the Ba stream sediment concentrations are all greater than the 50th percentile (i.e. > 533 ppm, yellow on Fig. 8) which contrasts with the ORS strata in the Anglo-Welsh Basin, where the majority of Ba stream sediment concentrations are below the 50th percentile range (i.e. below 533 ppm, green on Fig. 8) (Everett et al., 2019). There are high-Ba stream sediment concentrations (>942 ppm) in several locations in Caithness, in southwest Mainland Orkney and across Shetland. Orkney contains among the finest Neolithic settlements and monuments in the UK, including the Ring of Brodgar and the Stones of Stenness on Orkney, both constructed using ORS age sandstone identified as being quarried at Vestra Fiold and Staneyhill within a few kilometres of the stone circles (Richards, 2013).

On Orkney, the basement granites underlying (unconformably) the Old Red Sandstone in the southwest of Mainland have elevated Ba (Lundmark et al., 2019 and see Fig. 8), although the Ba anomaly in this area seems to relate to copper-uranium-rare earth element (plus baryte) mineralization linked to an exhumed oil reservoir (Heptinstall et al., 2023). In Shetland, high-Ba levels coincide with metamorphic and plutonic rocks underlying the Devonian Walls and Sandness formations (Melvin, 1985), which include, on Papa Stour, Shetland, some Middle Devonian volcanic sequences. Basalts in these sequences have vesicles infilled with baryte (up to 10 cm across as agate-baryte amygdalae), a testament to Ba-mobility in the basin during diagenesis of the Middle ORS (Mykura and Newsier, 1976). A baryte cement in the ORS of these areas may be expected and might account for the elevated stream sediment Ba.

Thomas (1923) divided the stones used in the construction of Stonehenge into two groups, namely the sarsens (of relatively local origin) and the 'foreign stones' or the 'blue stones' and he included the Altar Stone in his 'blue stone' group, hence assuming a common 'cultural' origin. In doing so he sought a provenance for the Altar Stone in west or south Wales, suggesting possible sources in the Cosheston Group around Milford Haven or possibly from somewhere in the outcrop of the Senni Beds in 'Glamorganshire' (now parts of the counties of Carmarthenshire, Powys and Monmouthshire). It is clear from his paper that he thought all of the bluestones were from a single source area in west or south Wales brought together within a unified effort.

This Wales source for the Altar Stone has remained unchallenged for almost a century. The Altar Stone has frequently been referred to as an anomalous bluestone, both in its lithology and in its size and weight. It is also not known when it arrived at Stonehenge (M. Pitts, pers. comm.). Parker Pearson (2023) considered that the bluestones (56 in number) were erected in the set of stone holes known as the Aubrey Holes during the Stage 1 construction phase (c. 2950 BCE). Because of its size the Altar Stone would have looked at odds amongst a ring of smaller bluestones so a possibility, to explain its anomalous characteristics, is that it arrived at a different time and from a different source area to the bluestones. 'Declassifying' the Altar Stone as a bluestone frees up thinking regarding a potential source for the stone and has led us to consider that it is an appropriate time to broaden our horizons, both geographically and stratigraphically in our search for the source of the Altar Stone. This is the next phase of our investigation, in which we will seek to try to match the distinctive lithology, mineralogy and geochemistry of the Altar Stone to Old Red Sandstone sequences across the other regions of Britain described above, considering also younger strata of Permian and Triassic age. We will be in part guided by tools such as the barium stream sediment distribution maps, but we will also endeavour to gain an understanding of the source provenance of the Altar Stone component minerals by extending the use of Raman Spectroscopy and also by age determinations of those minerals. We intend also to collaborate with archaeologists to explore the proposed long-distance links between Stonehenge and other regions of Britain, such as evidence that cattle and pigs feasted on at Durrington Walls were brought from western and northern areas, including Scotland (Madgwick et al., 2019, but see Evans et al., 2022). This long-distance connection occurred during the Stage 2 construction phase (c. 2500 BCE) so maybe the Altar Stone arrived

during this period, well after the bluestones were erected? The timing of these links needs to be further explored in order to try to discover when the Altar Stone arrived at Stonehenge. These considerations will inform the next phase of our investigations.

8. Conclusions

For the last 100 years the Stonehenge Altar Stone has been considered to have been derived from the Old Red Sandstone sequences of south Wales, in the Anglo-Welsh Basin, although no specific source location has been identified. Our extensive sampling, petrographic examinations, portable XRF analyses, automated SEM-EDS investigations and very preliminary Raman Spectroscopy have similarly failed to provenance the stone. Indeed, only four samples from our dataset have Ba levels comparable to those in the Altar Stone and more detailed investigations of those four samples discounts each sample and its location as being linked to the source of the stone. We have concluded that the Altar Stone appears not, in fact, to come from the ORS of the Anglo-Welsh Basin and further, we propose that the Altar Stone should no longer be included in the “bluestone” grouping of rocks essentially sourced from the Mynydd Preseli. Accordingly, in our on-going pursuit of the provenance of the Altar Stone we consider it time to broaden horizons, both geographically and stratigraphically, to include parts of Britain with evidence of Neolithic peoples and their monuments. Attention will now turn to the ORS of the Midland Valley and Orcadian Basins in Scotland as well as Permian-Triassic of northern England to ascertain whether any of these sandstones have a mineralogy and geochemistry which match the Stonehenge Altar Stone.

Declaration of Competing Interest

The authors declare that they have no known competing financial interests or personal relationships that could have appeared to influence the work reported in this paper.

Data availability

Data submitted as [Supplementary tables](#)

Acknowledgements

Salisbury Museum and Amgueddfa Cymru – National Museum Wales are thanked for the loan of samples used in this study. We also thank Keith Ray and Jon Morris for assistance with the collection of field samples. The senior author acknowledges financial support for this work from the Leverhulme Trust through award of an Emeritus Fellowship. Finally, very helpful comments from two reviewers led to improvements in this contribution.

Appendix A. Supplementary data

Supplementary data to this article can be found online at <https://doi.org/10.1016/j.jasrep.2023.104215>.

References

- Andò, S., 2020. Gravimetric separation of heavy minerals in sediments and rocks. *Minerals* 10, 273. <https://doi.org/10.3390/min10030273>.
- Andò, S., Garzanti, E., 2013. Raman spectroscopy in heavy-mineral studies. In: Scott, R. A., Smyth, H.R., Morton, A.C., Richardson, N. (Eds.), *Sediment Provenance Studies in Hydrocarbon Exploration and Production*. Geological Society, London, Special Publications, pp. 395–412. <https://doi.org/10.1144/SP386.2>.
- Andò, S., Vignola, P., Garzanti, E., 2011. Raman counting: A new method to determine provenance of silt. *Rendiconti Lincei* 22, 327–347. <https://doi.org/10.1007/s12210-011-0142-4>.
- Barclay, W.J., Browne, M.A.E., McMillan, A.A., Pickett, E.A., Stone, P., Wilby, P.R. (Eds.), 2005. *The Old Red Sandstone of Great Britain*. Geological Conservation Review Series, No. 31. Joint Nature Conservation Committee, Peterborough, p. 393.
- Barclay, W.J., Davies, J.R., Hillier, R.D., Waters, R.A., 2015. *Lithostratigraphy of the Old Red Sandstone successions of the Anglo-Welsh Basin*. British Geological Survey Research Report RR/14/02, 96 pp.
- Bevins, R.E., Ixer, R.A., Webb, P.C., Watson, J.S., 2012. Provenancing the rhyolitic and dacitic components of the Stonehenge Landscape bluestone lithology: New petrographical and geochemical evidence. *J. Archaeol. Sci.* 39, 1005–1019. <https://doi.org/10.1016/j.jas.2011.11.020>.
- Bevins, R.E., Ixer, R.A., Pearce, N.J.G., 2014. Carn Goedog is the likely major source of Stonehenge doleritic bluestones: Evidence based on compatible element discrimination and principal component analysis. *J. Archaeol. Sci.* 42, 179–193. <https://doi.org/10.1016/j.jas.2013.11.009>.
- Bevins, R.E., Pirrie, D., Ixer, R.A., O'Brien, H., Pearson, M.P., Power, M.R., Shail, R.K., 2020. Constraining the provenance of the Stonehenge ‘Altar Stone’: Evidence from automated mineralogy and U-Pb zircon age dating. *J. Archaeol. Sci.* 120 <https://doi.org/10.1016/j.jas.2020.105188>.
- Bevins, R.E., Ixer, R.A., Pirrie, D., Power, M.R., Cotterell, T., Tindle, A.G., 2021. Alteration fabrics and mineralogy as provenance indicators; The Stonehenge bluestone dolerites and their enigmatic spots. *J. Archaeol. Sci. Rep.* 36 <https://doi.org/10.1016/j.jasrep.2021.102826>.
- Bevins, R.E., Pearce, N.J.G., Ixer, R.A., Hillier, S., Pirrie, D., Turner, P., 2022a. Linking derived debitage to the Stonehenge Altar Stone using portable X-ray fluorescence analysis. *Mineral. Mag.* 86, 688–700. <https://doi.org/10.11180/mgm.2022.22>.
- Bevins, R.E., Pearce, N.J.G., Parker-Pearson, M., Ixer, R.A., 2022b. Identification of the source of dolerites used at the Waun Mawn stone circle in the Mynydd Preseli, west Wales and implications for the proposed link with Stonehenge. *J. Archaeol. Sci. Rep.* 45 <https://doi.org/10.1016/j.jasrep.2022.103556>.
- Bevins, R.E., Pearce, N.J.G., Pirrie, D., Ixer, R.A., Hillier, S., Turner, P., Power, M.R., 2023. Assessing the authenticity of a sample taken from the Altar Stone at Stonehenge in 1844 using portable XRF and automated SEM-EDS. *J. Archaeol. Sci. Rep.* 49 <https://doi.org/10.1016/j.jasrep.2023.103973>.
- British Geological Survey, 1993. *Regional geochemistry of southern Scotland and part of northern England*. British Geological Survey, Keyworth, Nottingham.
- British Geological Survey, 2000. *Regional Geochemistry of Wales and part of West Central England: Sediment and Soil*. British Geological Survey, Keyworth, Nottingham.
- Colvine, R., 1995. *Regional Geochemistry of the Lake District and adjacent areas*. Geochemistry Group of the British Geological Survey, Keyworth, Nottingham (British Geological Survey), 1993. viii+ 98 pp, 46 coloured maps+ 1: 250 000 geological map.
- Cunnington, W., 1884. Stonehenge notes: The fragments. *Wiltshire Archaeological and Natural History Magazine* 21, 141–149.
- Darvill, T., 2022. Mythical rings? Waun Mawn and Stonehenge Stage 1. *Antiquity* 390 10.15184/aqy.2022.82.
- Downes, J., Richards, C., Brown, J., Creswell, A.J., Ellen, R., Davies, A.D., Hall, A., McCulloch, R., Sanderson, D.C.W., Simson, I.A., 2013. *Investigating the Great Ring of Brodgar*. In: Richards, C. (Ed.), *Building the Great Stone Circles of the North*. Oxbow Books, pp. 90–118.
- Evans, J.A., Pashley, V., Mee, K., Wagner, D., Parker Pearson, M., Fremondeau, D., Albarella, U., Madgwick, R., 2022. Applying lead (Pb) isotopes to explore mobility in humans and animals. *PLoS One* 17 (10), e0274831. <https://doi.org/10.1371/journal.pone.0274831>.
- Everett, P.A., Lister, T.R., Fordyce, F.M., Ferreira, A.M.P.J., Donald, A.W., Gowing, C.J. B., Lawley, R.S., 2019. *Stream sediment geochemical atlas of the United Kingdom, OR/18/048*. British Geological Survey 94.
- Forde-Johnston, J.L., 1958. *Megalithic art in the north-west of Britain: The calderstones*. Liverpool. Proc. Prehist. Soc. 23, 20–39.
- Garzanti, E., Andò, S., 2007a. Heavy-mineral concentration in modern sands: Implications for provenance interpretation. In: Mange, M.A. & Wright, D.T. (Eds.), *Heavy Minerals in Use*. Developments in Sedimentology Series, vol. 58, pp. 517–545.
- Garzanti, E., Andò, S., 2007b. Plate tectonics and heavy-mineral suites of modern sands. In: Mange, M.A. & Wright, D.T. (Eds.), *Heavy Minerals in Use*. Elsevier, Amsterdam, Developments in Sedimentology Series, vol. 58, pp. 741–763.
- GERM, 2021. *Geochemical Earth Reference Model (GERM) Partition Coefficient (Kd) Database*, <https://www.earthref.org/KDD/>.
- Heptinstall, E.A., Parnell, J., Armstrong, J.G.T., Schito, A., Akinsanpe, T.O., 2023. Copper, uranium and REE mineralisation in an exhumed oil reservoir, southwest Orkney. *Scotland. Geosciences* 13, 151.
- Hillier, S., Wilson, M.J., Merriman, R.J., 2006. Clay mineralogy of the Old Red Sandstone and Devonian sedimentary rocks of Wales. *Scotland and England. Clay Miner.* 41, 433–471.
- Hubert, J.F., 1962. A zircon-tourmaline-rutile maturity index and independence of composition of heavy mineral assemblages with gross composition and texture of sandstone. *J. Sediment. Petrol.* 32, 440–450.
- Ixer, R.A., Bevins, R.E., 2010. The petrography, affinity and provenance of lithics from the Cursus Field, Stonehenge. *Wiltshire Archaeological & Natural History Magazine* 103, 1–15.
- Ixer, R.A., Bevins, R.E., 2011. Craig Rhos-y-Felin, Pont Saeson is the dominant source of the Stonehenge rhyolitic debitage. *Archaeology in Wales* 50, 21–31.
- Ixer, R., Bevins, R., Turner, P., Power, M., Pirrie, D., 2019. *Alternative Altar Stones? Carbonate-cemented micaceous sandstones from the Stonehenge Landscape*. Wiltshire Archaeological and Nat. History Magazine 112, 1–13.
- Ixer, R.A., Bevins, R.E., Pirrie, D., Power, M., Webb, P., 2022. *Stonehenge Dacite Group D: Fact or fiction?* Wiltshire Archaeological & Nat. History Magazine 115, 117–132.
- Ixer, R.A., Bevins, R.E., Pirrie, D., Power, M., 2023. *Treasures in the attic*. Testing Cunnington’s assertion that Stone 32c is the ‘type’ sample for Andesite Group A. *Wiltshire Archaeology and Nat. History Magazine* 116, 1–15.

- Kendall, R.S., 2017. The Old Red Sandstone of Britain and Ireland — A review. *Proc. Geol. Assoc.* 128 (3), 409–421. <https://doi.org/10.1016/j.pgeola.2017.05.002>.
- Kretz, R., 1983. Symbols for rock forming minerals. *Am. Mineral.* 68, 277–279.
- Linares-Catela, J.A., Romero, T.D., Molina, C.M., Puro, L.M.C., 2023. Choosing the site, getting the stones, building the dolmens: Local sourcing of andesites at the El Pozuelo megalithic complex (Huelva, Spain). *Archaeol. Anthropol. Sci.* 15, 101. <https://doi.org/10.1007/s12520-023-01799-0>.
- Lundmark, A.M., Augland, L.E., Bjerga, A.D., 2019. Timing of strain partitioning and magmatism in the Scottish Scandian collision, evidence from the high Ba–Sr Orkney granite complex. *Scott. J. Geol.* 55, 21–34. <https://doi.org/10.1144/sjg2018-001>.
- Mange, A., Maurer, H.F.W., 1992. *Heavy minerals in colour*. Chapman and Hall, London, p. 147.
- Maskelyne, N.S., 1878. Stonehenge: The petrology of its stones. *Wiltshire Archaeological and Nat. History Magazine* 17, 147–160.
- Melvin, J., 1985. Walls Formation, western Shetland: Distal alluvial plain deposits within a tectonically active Devonian basin. *Scott. J. Geol.* 21, 23–40. <https://doi.org/10.1144/sjg21010023>.
- Mykura, W., Newsier, J., 1976. *The geology of western Shetland (Explanation of one-inch geological sheet western Shetland; comprising Sheet 127 and parts of 125, 126 and 128)*. Keyworth, Nottingham.
- Nash, D.J., Ciborowski, T.J.R., Ullyot, J.S., Parker Pearson, M., Darvill, T., Greaney, S., Maniatis, G., Whitaker, K.A., 2020. Origins of the sarsen megaliths at Stonehenge. *Sci. Adv.* 6 <https://doi.org/10.1126/sciadv.abc0133>.
- Parfenoff, A., Pomerol, C., Tourenq, J., 1970. *Minerals in grains: methods of study and determination*. Masson et Cie (Editeurs), 120, Boulevard Saint-Germain, Paris (6e), 550p.
- Parker Pearson, M., 2023. *Stonehenge: A brief history*. Bloomsbury Academic, p. 191 pp.
- Parker Pearson, M., Bevins, R.E., Ixer, R.A., Pollard, J., Richards, C., Welham, K., 2020. Long distance landscapes: from quarries to monument at Stonehenge. In: Boaventura, R., Mataloto, R., Pereira (Eds.), *Megaliths and Geology*. Archaeopress, Oxford, pp. 183–200.
- Pearce, N.J.G., Bevins, R.E., Ixer, R.A., 2022. Portable XRF investigation of Stonehenge bluestone 62 and potential source outcrops in the Mynydd Preseli, west Wales. *J. Archaeol. Sci. Rep.* 44 <https://doi.org/10.1016/j.jasrep.2022.103525>.
- Pirrie, D., Power, M.R., Rollinson, G.K., Wiltshire, P.E.J., Newberry, J., Campbell, H.E., 2009. Automated SEM-EDS (QEMSCAN) mineral analysis in forensic soil investigations; testing instrumental variability. In: Ritz, K., Dawson, L., Miller, D. (Eds.), *Criminal and Environmental Soil Forensics*. Springer, pp. 411–430.
- Pitts, M.W., 2022. *How to build Stonehenge*. Thames & Hudson Ltd, London, p. 240.
- Richards, C., 2013. *Building the Great Stone Circles of the North*. Oxbow Books, Building the Great Stone Circles of the North, p. 322.
- Richards, C., Brown, J., Jones, S., Hall, A., Muir, T., 2013. Monumental risk: megalithic quarrying at Staneyhill and Vestra Field, Mainland, Orkney. In: Richards, C. (Ed.), *Building the Great Stone Circles of the North*. Oxbow Books, pp. 119–148.
- Rollinson, H.R., Pease, V., 2021. *Using geochemical data: To understand geological processes*, 2nd edn. Cambridge University Press, Cambridge, p. 346.
- Sharpe, K.E., 2022. East of Eden: monumental rock art in Cumbria, England. In: Mazel, A., Nash, G. (Eds.), *Signalling and performance: Ancient rock art in Britain and Ireland*. Archaeopress Archaeology, pp. 96–121.
- Thomas, H.H., 1923. The source of the stones of Stonehenge. *Antiqu. J.* 3, 239–260. <https://doi.org/10.1017/S0003581500005096>.
- Thorpe, R.S., Williams-Thorpe, O., Jenkins, D.G., Watson, J.S. with contributions by Ixer, R.A., Thomas, R.G., 1991. The geological sources and transport of the bluestones of Stonehenge, Wiltshire, UK. *Proceedings of the Prehistoric Society*, 57, 103–157. <https://doi.org/10.1017/S0079497X00004527>.
- Zimmermann, U., Kristoffersen, E.S., Fredriksen, P.D., Bertolino, S.A.R., Andò, S., Bersani, D., 2016. Provenance and composition of unusually chrome and nickel-rich bucket-shaped pottery from Rogaland (southwestern Norway). *Sed. Geol.* 336, 183–196. <https://doi.org/10.1016/j.jsedgeo.2015.09.001>.